A Model for Characterizing Cortical Folding Patterns Across Species

Monica K. Hurdal and Deborah A. Striegel

Email: mhurdal@math.fsu.edu URL: www.math.fsu.edu/~mhurdal

Department of Mathematics, Florida State University, Tallahassee, Florida 32306-4510, U.S.A.

1. Introduction

The mechanisms for the formation of folding patterns of the cerebral cortex are still under debate. In the past ten years, with the discovery of intermediate progenitor (IP) cells, new hypotheses about how these folding patterns develop have been introduced. Here, we adopt the intermediate progenitor cell hypothesis [1] (IPH) and develop a new model of the production of IP cells using a Turing reaction-diffusion system. The domain for this model is a prolate spheroid based on the shape of the lateral ventricle.

We begin with the IPH and an example of Turing patterns on a one dimensional domain. We then expand Turing theory to predict evolving patterns on a prolate spheroidal surface. Next, we examine the role that focal distance plays in pattern formation and use it to predict the evolutionary development of cortical patterns in different species.

2. IPH of Cortical Development

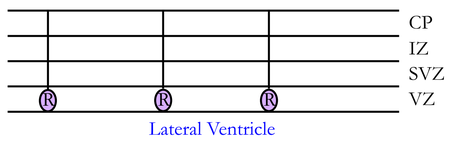

A founding population of radial glial cells (R) is created in the ventricular zone (VZ) which is located in the lateral wall of the lateral ventricle [2].

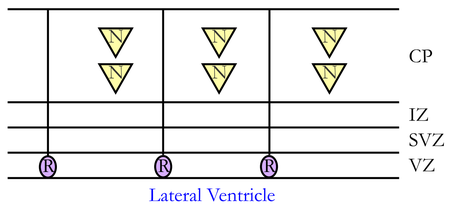

Radial glial cells (R) go through cycles of asymmetric cellular divisions creating neurons (N) that travel to the cortex creating the lower layers of the cortical plate (CP).

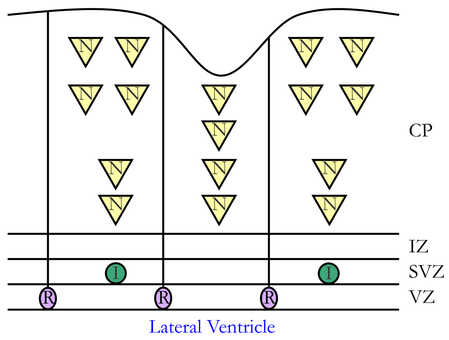

Select radial glial cells (R) switch to cycles of asymmetric cellular divisions creating IP cells (I) that travel to the subventricular zone (SVZ) and create two neurons (N) per cellular division that travel to the cortex. When a subset of "non-activated" radial glial cells is surrounded by subsets of "activated" radial glial cells a sulcus is formed [1].

Since the patterning of IP cells takes place in the VZ, we approximate the lateral ventricle with a prolate spheroid and the VZ with a prolate spheroidal surface.

3. Turing Systems

A Turing system is a reaction-diffusion system containing two morphogens, an activator $u(x,t)$ and an inhibitor $v(x,t)$ at position x and time t [3]. Turing systems have been used to describe pattern formation in a variety of biological and chemical systems.

The BVM (Barrio, Varea, and Maini) Turing System Model [4] is:

$$u_t = D\delta\nabla^2 u + \alpha u(1 - r_1 v^2) + v(1 - r_2 u),$$
$$v_t = \delta\nabla^2 v + \beta v\left(1 + \frac{\alpha r_1}{\beta} uv\right) + v(\gamma + r_2 u), \qquad (1)$$

where D is the ratio of diffusion coefficients, δ is inversely proportional to the domain scaling, and α, β, γ, r_1 and r_2 are kinetics parameters. Solutions to System 1 are of the form $u = T(t)X(x)$ where $T(t) = ce^{t\lambda(k^2)}$ and $\lambda(k^2)$ is the temporal eigenvalue and where $X(x)$ is a solution of $\nabla^2 X + k^2 X = 0$ [5].

4. Turing Patterns on a 1-D Domain

In one dimension, where $0 < x < P$ with a periodic boundary condition, the solution to $\nabla^2 X + k^2 X = 0$ is $X_k = A_k \cos(kx)$ and $k^2 = \left(\frac{n\pi}{P}\right)^2$ where n is an integer.

Diffusion driven instability, which leads to pattern formation, is accomplished when $\mathrm{Re}(\lambda(k^2)) > 0$. The associated k^2-values predict which pattern forms. Fig. 1 demonstrates the effect of domain scaling on pattern formation.

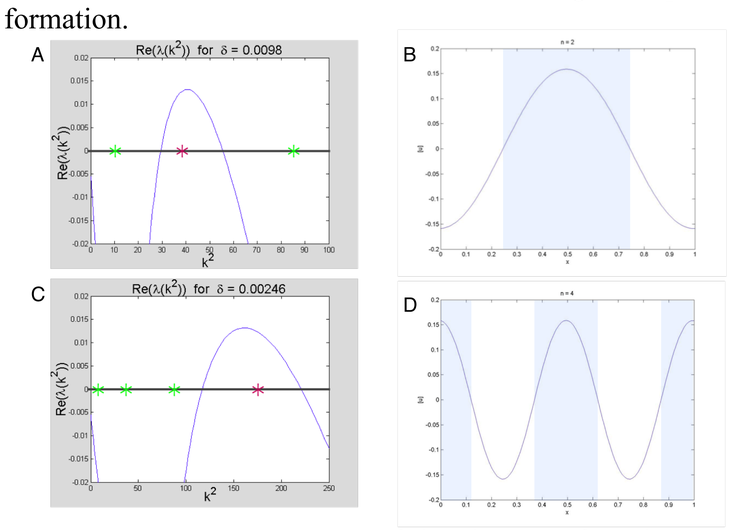

Fig. 1: Pattern Formation in 1D. Left (A, C): Pattern formation occurs when $\mathrm{Re}(\lambda(k^2)) > 0$. Right (B, D): Simulations of the distribution of u on the domain illustrate the observed pattern. Any x-value where $u > 0$ will be activated. **A)** The asterisks indicate the values for k^2 when $n = 1$, 2 and 3. The k^2 value in red (corresponding to $n = 2$) determines the pattern formed. **B)** Simulations reveal one region is activated (shaded blue). **C & D)** An increase in domain scaling (corresponding to a decrease in δ) results in a shift of the $\mathrm{Re}(\lambda(k^2))$ parabola. Now a larger k^2 value (indicated by red asterisk, corresponding to $n = 4$) is responsible for the resulting pattern (shaded blue). Parameter values: $D = 0.516$, $r_1 = 3.5$, $r_2 = 0$, $\alpha = 0.899$, $\beta = -0.91$, $\gamma = -0.899$, $P = 1$.

5. Prolate Spheroidal Surface Model

A prolate spheroid is obtained by rotating an ellipse on its major axis and has coordinates (ξ, η, φ) where ξ is the radial term, $\eta = \cos(\theta)$ with θ the polar angle, and φ is the angle of rotation. As above, $X(x)$ forms part of the solution to System 1. Since $X(x)$ is separable in prolate spheroidal coordinates [6], we can rewrite X in terms of

$$X_{mn} = R_{mn}(c,\xi)S_{mn}(c,\eta)\Phi_{mn}(\varphi)$$

where $c = \frac{1}{2}kf$, f = focal distance, (m,n) are the prolate spheroidal harmonic indices, and R, S and Φ satisfy

$$\frac{d}{d\xi}\left[(\xi^2 - 1)\frac{d}{d\xi}R_{mn}(c,\xi)\right] - \left[\lambda_{mn} - c^2\xi^2 + \frac{m^2}{\xi^2 - 1}\right]R_{mn}(c,\xi) = 0,$$

$$\frac{d}{d\eta}\left[(1 - \eta^2)\frac{d}{d\eta}S_{mn}(c,\eta)\right] + \left[\lambda_{mn} - c^2\eta^2 - \frac{m^2}{1 - \eta^2}\right]S_{mn}(c,\eta) = 0,$$

$$\Phi'' + m^2\Phi = 0.$$

Since the domain is a prolate spheroidal surface, the solution is radially invariant, i.e. $\frac{dR}{d\xi} = 0$, and we obtain Equation 2 to relate k^2 with the (m,n) pattern obtained [7],

$$k^2 = \frac{4}{f^2\xi_0^2}\left(\rho_{mn}\left(\frac{1}{2}kf\right) + \frac{m^2}{\xi_0^2 - 1}\right), \qquad (2)$$

where ξ_0 conserves a surface area of 4π and ρ_{mn} is a separation constant. Equation 2 will be denoted as A_{mn}, i.e.

$$A_{mn} = \frac{4}{f^2\xi_0^2}\left(\rho_{mn}\left(\frac{1}{2}kf\right) + \frac{m^2}{\xi_0^2 - 1}\right).$$

Mutations of a number of genes in mice have been shown to increase the production of IP cells [8]. Thus it is not unreasonable to assume that there is an activator located in the VZ that controls the creation of IP cells, leading to sulcus formation.

References and Further Information

1. A. Kriegstein, S. Noctor, V. Martinez-Cerdeno, *Nat Rev Neurosci*, **7(11)**, 883-890, 2006.
2. P. Rakic, *Science* **241(4962)**, 170-176, 1988.
3. A. M. Turing, *Philos T R Soc Lond B*, **237**, 37-72, 1952.
4. R. A. Barrio, C. Varea, J. L. Aragon, P. K. Maini, *B Math Biol*, **61(3)**, 483-505, 1999.
5. J. D. Murray, *Mathematical Biology*, 2nd ed., Springer, New York, 1989.
6. C. Flammer, *Spheroidal Wave Functions,* Stanford Univ. Press, Palo Alto, 1957.
7. D. A. Streigel, M. K. Hurdal, *PLoS Comput Biol*, **5(9),** e1000524, 2009.
8. A. Pontious, T. Kowalczyk, C. Englund, R. F. Hevner, *Dev Neurosci*, **30(1-3)**, 24-32, 2008.
9. J. Reighard, H. S. Jennings, *Anatomy of the Cat*, 3rd ed., Holt, Rinehart and Winston, New York, 1935.
10. K. Brodmann, *Brodmann's Localisation in the Cerebral Cortex*, 3rd ed., Springer, New York, 2006.

For further information please contact *mhurdal@math.fsu.edu*

For information on related projects please see *http://www.math.fsu.edu/~mhurdal*

6. Prolate Spheroidal Surface Patterns

With a fixed focal distance f, a graph of A_{mn} (the right hand side of Equation 2) versus k can be plotted for each (m,n). Fig. 2 shows two simulations on a prolate spheroidal surface (with focal distance $f = 1$). The top simulation (Figs. 2B and 2C) has a domain scaling corresponding to $k^2 = 30$. Notice, $k^2 = 30$ (lower asterisk in Fig. 2A) corresponds to curve A_{35} and verifies the (3,5) pattern obtained. The bottom simulation (Figs. 2C and 2D) corresponds to $k^2 = 60$ (top asterisk in Fig. 2A) and verifies the pattern predicted of A_{77}.

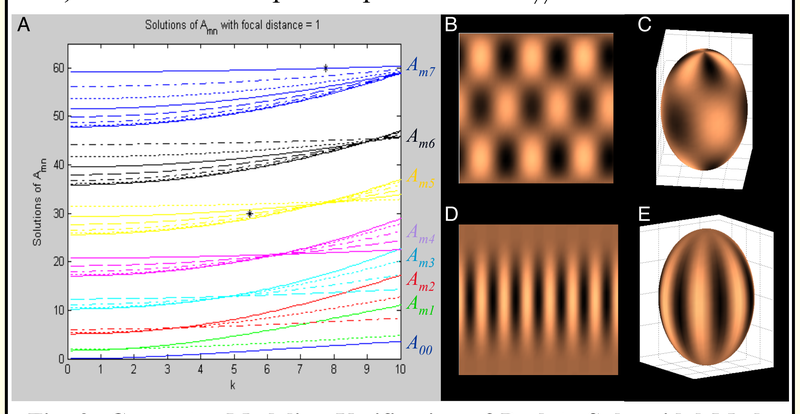

Fig. 2: Computer Modeling Verification of Prolate Spheroidal Mode Equation (Equation 2). A) Graph of A_{mn} for $n = 0, \ldots, 7$ (different colors) and $m = 0, \ldots, n$ (different linestyles, beginning with $m = 0$ on the bottom and $m = n$ on top) . When $k^2 = 30$ and 60 (bottom and top asterisks respectively) the corresponding patterns are A_{35} and A_{77} respectively. **B)** Results of discretization of BVM system for $\delta = 0.013$ (corresponding to $k^2 = 30$), $\alpha = 0.899$, $\beta = -0.91$, $\gamma = -0.899$, $D = 0.5319$, $r_1 = 3.5$, and $r_2 = 0$. **C)** Projection of Fig. B onto a prolate spheroidal surface ($f = 1$) such that top (bottom) edge maps to the north (south) pole of the spheroid. **D & E)** Same as Figs. B & C except $\delta = 0.0065$ (corresponding to $k^2 = 60$).

7. Evolutionary Development

Evolutionarily the cerebral cortex and lateral ventricle have expanded greatly. The expansion of the lateral ventricle is captured with the focal distance, f, of the prolate spheroid. Figure 3 shows plots of the curves A_{11}, A_{02}, and A_{04}. The pattern A_{11} corresponds to the pattern needed to create one sectorial sulcus (following along the major axis of the lateral ventricle). Curve A_{02} corresponds to one transverse sulcus forming a ring around the lateral ventricle and curve A_{04} corresponds to two transverse sulcal rings.

Notice in Fig. 3A that as k^2 increases, the first pattern it intersects is A_{11}. If f is increased (Fig. 3B), the curves shift and now as k^2 increases it intersects A_{02} before A_{11}; therefore one transverse sulcus could form before a sectorial sulcus. If f is increased further (Fig. 3C), as k^2 increases it intersects A_{04} before A_{11}, meaning two transverse sulci could form before the first sectorial sulcus. These scenarios are similar to what occurs in the cat, lemur, and human (see Figs. 3D-3E).

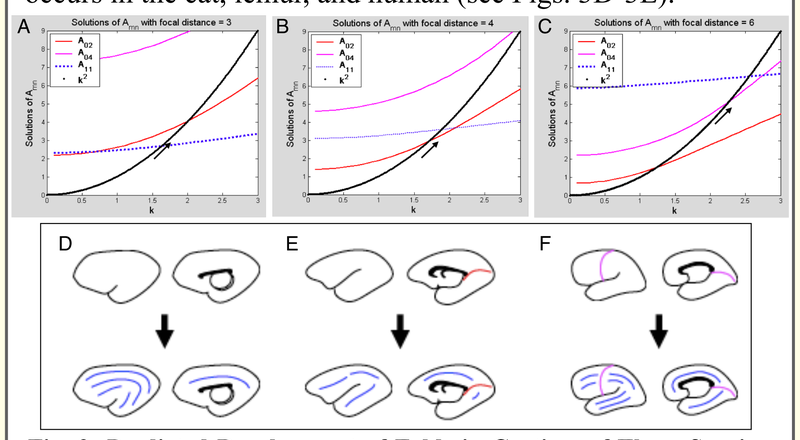

Fig. 3: Predicted Development of Folds in Cortices of Three Species. Top (A - C): As focal distance, f, increases, the order in which sulci form is predicted to change. **A)** When $f = 3$, an A_{11} pattern (one sectoral sulcus) is predicted to occur first. **B)** When $f = 4$, an A_{02} pattern forms before an A_{11} pattern, meaning one transverse sulcus could form before a sectorial sulcus. **C)** When $f = 6$, an A_{04} pattern forms before A_{11} meaning two transverse sulci could form before the first sectorial sulcus. Bottom (D – F): The top row shows the formation of transverse sulcal rings. The bottom row shows the subsequent creation of a certain number of sectorial sulci for **D)** Cat (modified from [9]), **E)** Lemur (modified from [10]), **F)** Human (modified from [10]).

8. Conclusions

Our model incorporates shape information of the lateral ventricle with the focal distance parameter of a prolate spheroid. Our model illustrates how sulcal placement and directionality are affected by changes in lateral ventricular eccentricity and predicts the development of the initial sulcal folds. The beauty of our model is that it provides an uncomplicated approach that relates to a biologically plausible mechanism of pattern formation.